Chemical Engineering Journal 543 (2026) 178541

Contents lists available at ScienceDirect

Chemical Engineering Journal

journal homepage: www.elsevier.com/locate/cej

A machine learning-assisted multi-criteria decision making framework for chemical reactor channel geometry selection

Mertcan Kaya [a,*], Jean-Luc Göttsche [a], Christoph Klahn [a,b]

[a] Karlsruhe Institute of Technology (KIT), Institute for Micro Process Engineering (IMVT), 76344 Eggenstein-Leopoldshafen, Germany
[b] Karlsruhe Institute of Technology (KIT), Institute of Mechanical Process Engineering and Mechanics (MVM), 76131 Karlsruhe, Germany

ARTICLE INFO

Dataset link: Supplement (Original data), Supplementary Data (Original data)

Keywords:
Machine learning
Chemical engineering
Additive manufacturing
Reactor development
Methanol synthesis
Energy storage

ABSTRACT

Additive manufacturing enables the realization of diverse and complex reactor channel geometries, substantially increasing the number of feasible design variants. While this design freedom offers opportunities for improved performance, it also complicates the systematic selection of geometries suitable for a given application. This paper presents a data-driven framework to support this selection process in the early reactor concept design phase. The framework employs surrogate models to predict key physical characteristics such as heat transfer, radial temperature difference, pressure drop, and flow profile, and integrates these into a multi-criteria decision making method to guide process engineers in selecting appropriate channel geometries. By focusing on fundamental physical characteristics rather than reaction-specific results, the framework ensures that the surrogate models remain transferable across different reaction systems. Incorporating probabilistic dimensioning further narrows the solution space and reduces the need for iterative experimental campaigns or computationally demanding simulations in reactor design. The applicability of the proposed framework is demonstrated through two case studies in methanol synthesis, highlighting its potential to streamline early-stage reactor development.

1. Introduction

Additive manufacturing (AM) is gaining traction in the chemical industry due to its potential to enhance heat and mass transfer, improve mechanical stability for high pressure applications, and enable process intensification [1,2]. These capabilities are particularly advantageous under the demanding conditions of flow chemistry and in the miniaturization of reactor systems, such as those used in decentralized e-fuel production. In recent years, various novel reactor geometries have been proposed to exploit these benefits [3–7].

As novel design principles expand the available reactor design space, selecting the most suitable geometry for a given application becomes increasingly challenging. As Otto and Antonsson note, optimal solutions in engineering design often require trade-offs between fundamentally different concepts to best satisfy overall design objectives and preferences [8]. In the context of chemical engineering, for example, microchannel structures can substantially enhance heat transfer due to their large surface-area-to-volume ratio, but their small hydraulic diameter leads to a steep increase in pressure drop [9]. Depending on the process requirements, this pressure drop may become a limiting factor, underscoring the importance of carefully balancing competing design criteria during geometry selection.

The challenge of selecting an optimal design geometry has been extensively investigated within the domain of product development and is systematically addressed in established engineering design methodologies. For instance, the VDI 2221 guideline underscores balancing competing requirements during selection and refinement of design geometries, recommending initiation of this process in the early phases of product development [10]. In practice, the generation of potential geometries are often supported by structured brainstorming sessions, morphological analysis, and creativity-enhancing methods such as TRIZ, which are designed to systematically explore and resolve design contradictions [11]. The evaluation and selection of alternative geometries are typically supported by multi-criteria decision making (MCDM) techniques, which enable a structured comparison of design options across multiple, often conflicting, objectives and constraints. MCDM generally involves two stages: a multi-objective optimization (MOO) step to identify trade-offs between competing goals, followed by a decision making step to select the most suitable geometry based on application-specific priorities [12,13].

While these methods offer a formalized structure, they still depend on expert judgment for evaluating design performance, which can make the outcome sensitive to the designer's experience, particularly

* Corresponding author.
E-mail address: mertcan.kaya@kit.edu (M. Kaya).

https://doi.org/10.1016/j.cej.2026.178541
Received 12 March 2026; Received in revised form 15 May 2026; Accepted 17 June 2026
Available online 22 June 2026

in chemical reactor engineering. This reliance is largely a consequence of the limited availability of data representing real reactor behavior and the demanding conditions required to obtain reliable experimental measurements. For instance, the characterization of chemical reactors often requires sophisticated setups and is both time- and cost-intensive due to elevated pressures, high temperatures, and reaction-specific configurations. Consequently, recent studies have increasingly turned to numerical simulations and high-fidelity modeling to generate simulation data that approximate reactor behavior under varying conditions [7,14]. Although simulations reduce the experimental effort needed to navigate the AM-broadened reactor design space, they remain contingent on application-specific boundary conditions and must be validated experimentally. Moreover, the resulting datasets are typically valid only for the specific application they were generated for. When the design objective or operating conditions shift, new simulations and their corresponding experimental validations are necessary, which continues to pose a significant challenge for efficient and flexible reactor design.

Importantly, detailed simulations and experimental validations are typically conducted during the later phases of product development, known as deterministic design, once the geometry has already been selected and the design has been largely defined. As a result, the opportunity to explore and compare alternative geometries early in the design process remains limited. This limitation becomes particularly pronounced in the context of reactor design, where the solution space is extensive, and deterministic approaches quickly become impractical. To address this challenge, probabilistic design provides a complementary strategy by incorporating domain-specific statistical knowledge of uncertainties to estimate the likelihood of performance requirement violations [15,16]. This enables a more robust basis for making informed design decisions early in the reactor development, where choices have the greatest impact on performance and cost. Building on this idea, this paper introduces a data-driven framework for channel geometry selection, integrating surrogate modeling with structured decision making, specifically tailored to the design of methanol synthesis reactors. The proposed framework supports chemical reactor designers by partially automating the selection process and providing a probabilistic evaluation of channel geometry candidates, weighted according to user-defined priority criteria. Furthermore, the framework establishes a flexible and scalable foundation for future automation efforts, capable of accommodating increasingly complex reactor design tasks. The key contributions of this paper are as follows:

- Development of a data-driven framework to support channel geometry selection in chemical reactor design.
- Enabling reliable probabilistic decision making in the early stages of reactor development using limited experimental data.
- Providing a cost-effective solution to assist the design decision making process under uncertainty.
- Demonstration and validation of the proposed framework through two representative case study.

This paper is structured as follows: Section 2 provides a comprehensive review of the state of the art in decision making methods for geometry selection, highlighting the motivation for a data-driven framework. Section 3 introduces the proposed data-driven framework for reactor channel geometry selection in the early stages of reactor development, demonstrated for the case of methanol synthesis reactor design. Section 4 discusses the results, evaluating the effectiveness of the framework and illustrating its practical applicability.

2. State of the art

2.1. Geometry selection in reactor development

In classical chemical reactor engineering, the selection of the reactor type, such as batch reactors (BR), plug flow reactors (PFR), or continuous stirred tank reactors (CSTR), plays a critical role and is well established through mathematical modeling. The appropriate choice depends on the specific characteristics of the reaction, such as kinetics, heat and mass transfer requirements and operational constraints, which directly influence the mixing behavior and the resulting distribution of residence time, temperature, pressure, and concentration within the reactor volume [17–19]. However, reactor design is not solely limited to selecting the reactor type. While the choice between BR, PFR or CSTR has traditionally received primary attention, the selection of reactor channel geometry is becoming equally important. This shift is driven by the growing availability of AM, which enable the realization of complex and non-conventional geometries. As a result, for a given reactor type, such as a PFR, numerous geometry variants can now be designed and used to increase the reaction efficiency. For example, Magnanelli et al. demonstrated that a nature-inspired PFR channel design achieved an 11% reduction in total entropy production compared to a conventional cylindrical configuration in the catalytic oxidation of sulfur dioxide [20]. Similarly, Cho et al. developed a lung-inspired geometry for fuel cell channels, which improved reactant distribution and concentration homogeneity upstream of the catalyst layer, thereby enhancing overall fuel cell performance [21]. In the context of methanol synthesis, our previous works have demonstrated the importance of accounting for reactor channel geometry in the early stages of reactor development, particularly as a means to reduce computational demands in automated reactor design workflows [22,23].

As Dash et al. emphasize, the design selection of microchannels is critical and must account for factors such as heat transfer, pressure drops, manufacturability and overall practicality [24]. These factors are also critical in the context of methanol synthesis. Owing to the exothermic nature of the reaction, the literature emphasizes the importance of maintaining near-isothermal conditions within the reactor [25,26]. A rapid temperature rise can impair catalyst activation and thereby limit the achievable methanol yield [27,28]. Pressure is another decisive factor, as high operating pressures combined with plug flow behavior shift the equilibrium toward methanol formation, increasing conversion [29]. However, these factors are interdependent and often involve trade-offs. To address this complexity, Krishna and Sie proposed distinguishing between “process musts” and “process wants” during reactor geometry selection. While “musts” refer to essential criteria such as safe operation, suitable pressure and temperature ranges, environmental compliance and scalability, “wants” include desirable attributes like high conversion, simple operation and cost efficiency [30,31]. Given the increasing variety of feasible geometries enabled by AM, a systematic decision making approach that incorporates both required and preferred criteria is essential for reactor channel geometry selection. Such an approach ensures that the chosen design aligns with specific performance requirements and operational limitations of the intended application. However, despite its critical influence on reactor performance, channel geometry selection remains underexplored.

2.2. Multi-criteria decision making

Selecting an appropriate reactor channel geometry at the conceptual stage involves navigating multiple, and sometimes conflicting, design objectives and constraints. MCDM methods provide a structured and transparent framework for evaluating and ranking such alternatives. These methods enable the integration of both quantitative and qualitative criteria, facilitating informed and traceable design decisions. Widely used techniques include the Analytic Hierarchy Process (AHP), which supports hierarchical structuring and pairwise comparisons of decision criteria, the Technique for Order Preference by Similarity to Ideal Solution (TOPSIS), which ranks alternatives based on their proximity to ideal solutions and the Preference Ranking Organization Method for Enrichment Evaluations (PROMETHEE), which uses outranking techniques to accommodate both quantitative and qualitative inputs [32–34].

Fig. 1. General implementation steps of MCDM methods [35].

The general implementation of MCDM can be structured into three main steps (see Fig. 1). First, the decision problem must be thoroughly analyzed to identify the objectives, constraints and potential conflicts among the evaluation criteria. Given the inherent nature of multi-criteria decision problems, a single ideal solution rarely exists. Instead, the goal is to obtain a set of non-dominated and efficient solutions from the solution space. These solutions represent optimal trade-offs, where no improvement in one criterion can be achieved without compromising another [35,36]. Consequently, understanding the trade-offs within the system is crucial, and the relative importance of each criterion must be carefully established through appropriate weighting methods. In the final step, a suitable MCDM method must be selected and applied to rank the available alternatives according to the established criteria and weights. As an example, TOPSIS identifies the best alternative by evaluating the geometric distance of each option from an ideal solution. Alternatives are ranked based on their proximity to the ideal solution, with a higher rank assigned to options that have the shortest distance to the positive ideal solution and the farthest distance from the negative ideal solution. The general stepwise procedure and mathematical formulation of TOPSIS are described in [37,38]. The specific implementation adopted in this study is additionally provided in the Supplementary Information.

MCDM methods are broadly applied in engineering design. Xiaomin et al. integrated AHP into the conceptual design process for a bionic fan blade [39]. Youssef and Webster applied PROMETHEE to support decision making in the development of a diagnostic system [40]. To the best of our knowledge, MCDM methods have not yet been applied to the specific problem of reactor channel geometry selection. They are widely used in chemical and process engineering, especially in process design and system layout. Nabavi et al. combined MCDM with optimization to identify optimal process parameters for a multitubular membrane reactor designed for ethylene production [41]. In another application, MCDM methods have supported decision making in decentralized energy systems, particularly for isolated regions such as islands, where alternatives are evaluated based on cost and feasibility criteria [42].

2.3. Machine learning usage within MCDM

Since understanding the trade-offs within the system is critical, the availability of accurate and representative data for the specific case is essential. To address limitations in data quality or availability, recent studies have integrated machine learning (ML) techniques within MCDM methods [43–47]. ML-assisted MCDM approaches can enhance decision making by learning patterns, approximating missing data, or generating reliable surrogate models. For example, Nabavi et al. developed an artificial neural network model to predict reaction rates with high accuracy and reduced computational cost. The outputs of this model were then incorporated into the decision making process for optimizing a steam methane reforming reactor [45]. In another study, Wang et al. demonstrated the applicability of various ML algorithms, including random forests, support vector machines, multilayer perceptron neural networks and gradient boosting models, across two chemical engineering case studies to support informed and efficient decision making [43].

The integration of ML models within MCDM frameworks is typically oriented toward solving supervised regression problems, where the objective is to predict continuous performance metrics based on a set of input variables. To address these problems, models such as random forest regressors, artificial neural networks, support vector regression and gradient boosting machines are commonly employed, as they are capable of capturing complex nonlinear relationships between design variables and performance outcomes. Once trained, these models can efficiently generate accurate predictions across a wide solution space, thereby enabling the construction of a comprehensive multi-criteria decision matrix. This matrix serves as the basis for applying MCDM methods to rank and select the most suitable alternatives according to multiple performance indicators.

To ensure the reliability of ML-assisted decisions, the predictive accuracy of the surrogate models must be rigorously evaluated. Common metrics for regression model evaluation include the coefficient of determination (R^2), mean squared error (MSE), mean absolute error (MAE) and root mean squared error (RMSE) [44,46,48]. In this work, we used the following equations to evaluate ML model performance metrics:

$$R^2 = 1 - \frac{\sum_{i=1}^{n}(y_i - \hat{y}_i)^2}{\sum_{i=1}^{n}(y_i - \bar{y})^2} \tag{1}$$

$$\mathrm{RMSE} = \sqrt{\frac{1}{n}\sum_{i=1}^{n}(y_i - \hat{y}_i)^2} \tag{2}$$

In the above equations, y_i denotes the actual value at data point i and $\hat{y}_i$ represents the predicted value at the same point, obtained from the ML model. The term $\bar{y}$ is the mean of all actual values, calculated as $\bar{y} = \frac{1}{n}\sum_{i=1}^{n} y_i$ and n is the total number of data points in the dataset. The coefficient of determination R^2 indicates the proportion of variance in the dependent variable that is predictable from the independent variables. A value closer to 1 implies a better model fit. The RMSE quantifies the average magnitude of the prediction error by taking the square root of the mean of the squared differences between actual and predicted values. It retains the same units as the target variable, making it intuitively interpretable in the context of the original data. Lower RMSE values indicate better model performance, with smaller errors between predicted and actual outcomes [48–50].

3. Proposed framework for reactor channel geometry selection

This paper introduces a data-driven framework integrating probabilistic reasoning to systematically select reactor channel geometries. The framework development addresses the following key requirements:

- **Data-driven decision making framework:** The framework relies on real system response rather than solely on expert judgment, enabling objective comparisons among alternative channel designs and reducing subjective biases in decision making.
- **Use of general data applicable to different applications:** The framework employs generalized physical data applicable across various reactor types, ensuring broad utility. As a result, the generated datasets are reaction-independent and can be reused across multiple reaction systems, thereby minimizing the effort required for data generation.
- **Time- and cost-efficient data generation:** The framework employs efficient methodologies for generating experimental and simulation data, allowing extensive exploration of the solution space without incurring excessive costs or long lead times.
- **Partially automated geometry selection:** The framework supports reactor designer involvement through partial automation, while also providing capability for fully automated decision making when desired.

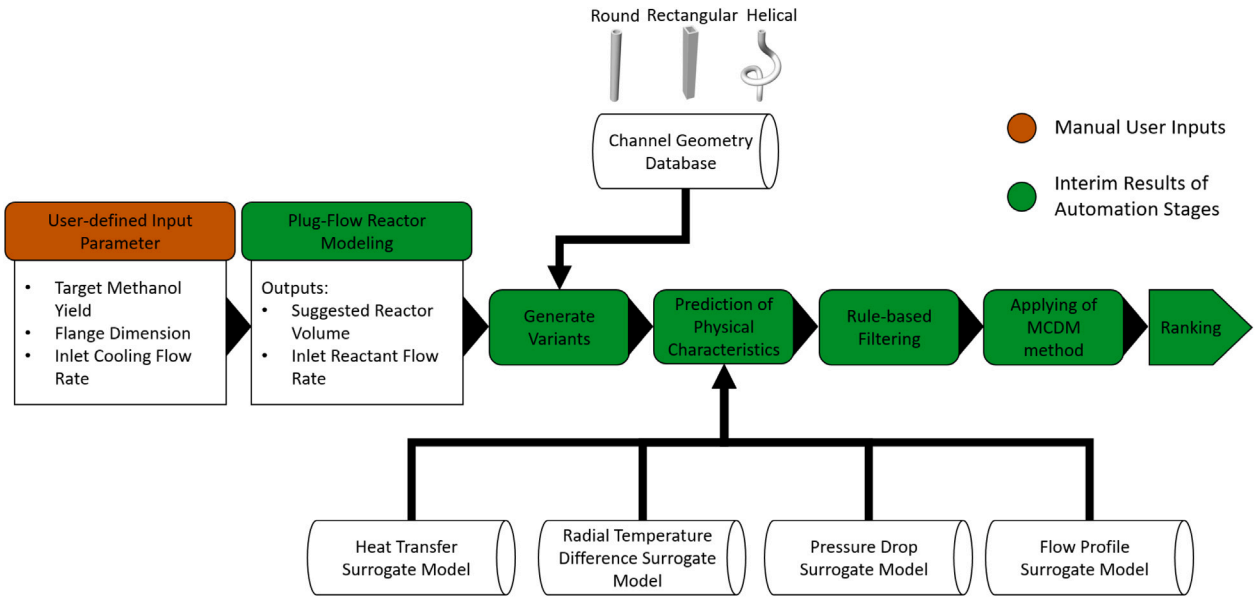

Fig. 2. Data-driven framework with its steps for reactor channel geometry selection.

To fulfill these requirements, the proposed framework focuses on the systematic generation and comparison of channel geometry variants in packed-bed PFR for methanol synthesis, where internal structures significantly influence reactor performance. Three representative geometries, round, rectangular and helical, were selected for this study, as they represent the most common channel geometries used in reactor and heat-transfer applications. To limit the number of variants in the experimental work, the geometrical variation is restricted to channel size and channel length. For the rectangular geometry, a fixed aspect ratio of 1.5 between channel width and height is applied. Although this restriction narrows the range of channel variants, it provides a clear demonstration of the framework within reactor development.

Based on these configurations, the framework operates by first defining input parameters, which are application-specific and depend on the reaction system and operational requirements. Subsequently, the reactor volume required to reach the target conversion is determined using an analytical calculation for methanol synthesis based on an ideal PFR model applied to the reference round channels within a classical multitubular reactor configuration. In this implementation, the reaction rates are calculated using the kinetic model reported in [51]. The PFR calculation assumes steady-state operation, one dimensional flow along the reactor axis, negligible axial dispersion, and uniform radial temperature and concentration profiles [52,53]. An example of this calculation is provided through the analytical PFR implementation available on GitHub [54], while the application of the PFR model is described in detail in our earlier work [23]. Based on the resulting reference reactor volume, alternative geometry variants with equivalent reactor volumes are generated using the database and evaluated based on their general physical characteristics (see Fig. 2). The use of generalized physical characteristics, rather than reaction-specific data, enables a consistent and transferable evaluation framework applicable across diverse reactions. The central idea is to employ a common set of physical descriptors independent of specific reaction kinetics, as reactor design is primarily governed by transport phenomena and thermodynamic constraints rather than reaction kinetics [55]. These physical descriptors are used to compare different geometrical variants, thereby substantially reducing the additional experimental and computational effort required to evaluate reactor designs with different channel configurations. As highlighted in Section 2.1, the appropriateness of a reactor design for methanol synthesis is primarily determined by physical parameters such as the distribution of residence time, temperature and pressure control within the reactor volume. To capture these aspects, we define four key physical characteristics, namely heat transfer, radial temperature difference, pressure drop, and flow profile. These characteristics are selected because they represent the main ways in which channel geometry affects methanol synthesis performance, namely heat removal, temperature uniformity, pressure loss, and residence-time behavior. Other characteristics, such as safe operation, environmental compliance, and scalability, are not introduced as separate criteria in this study because they require a deterministic assessment of the complete reactor design rather than a probabilistic preselection of individual channel geometries. However, the framework is extensible and can incorporate additional characteristics when required for a specific application. Surrogate models are trained to predict the physical characteristics for each generated geometrical variant of the considered channel geometries. Based on these predictions, a rule-based filtering step is first applied to eliminate non-viable variants. The remaining variants are then evaluated using a MCDM process and ranked accordingly. Following the MCDM evaluation, the framework suggests channel geometry variants, including their dimensions and length, together with efficiency percentages that guide the designer toward the final selection. Through this process, the framework enables probabilistic evaluation and systematic comparison of channel geometry variants in the early stages of methanol synthesis reactor design. The following subsections provide a detailed description of the physical data generation, the prediction of physical characteristics, and the decision making model for reactor channel geometry selection.

3.1. Physical data generation

Accurate ML prediction of the physical behavior associated with a given channel geometry requires a sufficiently large dataset obtained through experimental measurements or high-fidelity numerical simulations. In this study, a hybrid data generation approach is adopted, combining both experimental and simulation data to characterize four key physical parameters: heat transfer, radial temperature difference, pressure drop, and flow profile. For each parameter, simplified test specimens are specifically designed to facilitate experimental data collection. In cases where the experimental dataset is insufficient for constructing reliable surrogate models, numerical simulation results are used to supplement the data. Two CFD simulation models are developed to obtain the relevant physical characteristics and are validated against the experimental measurements. The first model simulates the heat transfer behavior within a packed-bed channel, replicating the

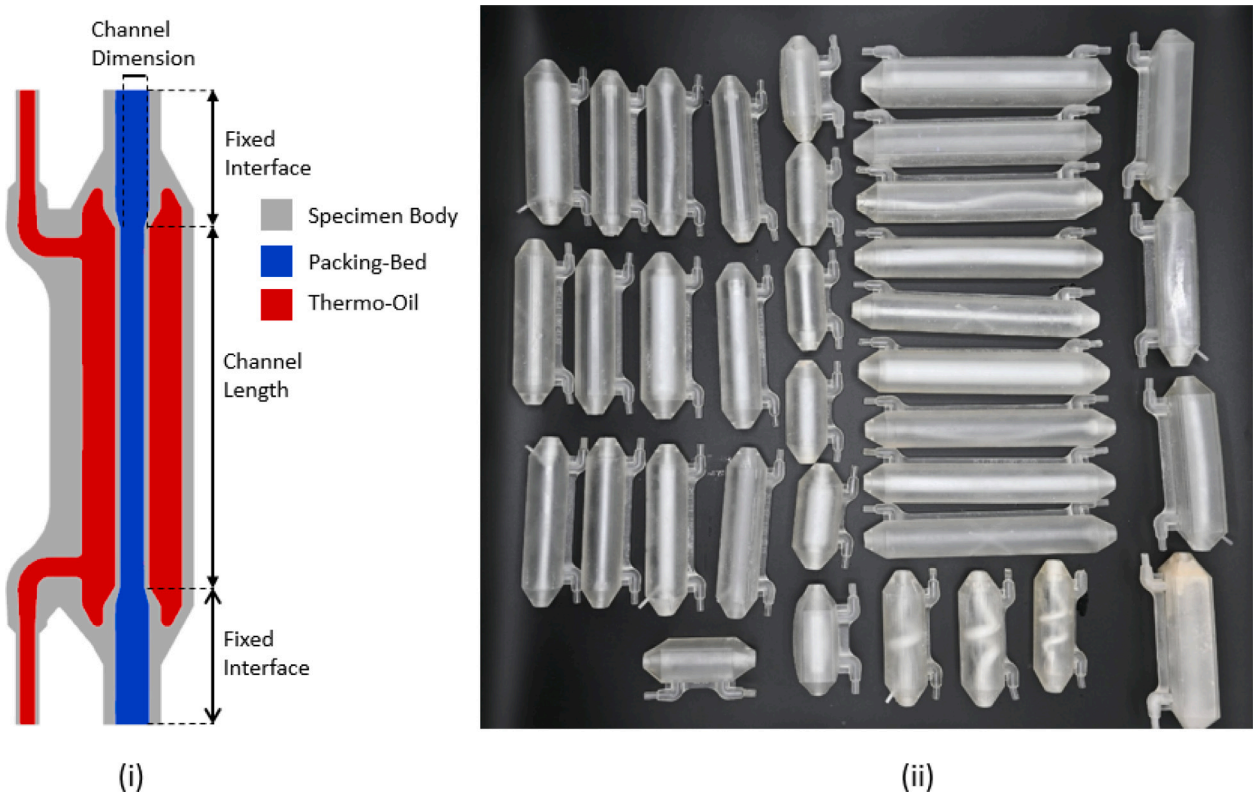

Fig. 3. (i) Example of a test specimen design for heat transfer experiments with remarked parameters; (ii) overview of the manufactured parts used for physical characterization.

experimental geometry and accounting for the effects of a surrounding cooling fluid. This simulation provides both the radial temperature difference and the heat transfer coefficient, including the thermal interactions at the wall. The second model focuses on fluid dynamics and is used to evaluate the pressure drop across the packed-bed channel. From this simulation, both the pressure difference and the maximum axial flow velocity difference along the channel are extracted. Given the large number of design parameters, including channel length, diameter, and flow rate, the resulting solution space comprises numerous possible configurations that must be adequately explored. A total of 83 experimental data points were generated and complemented with simulation data to train the surrogate models. Detailed information on the CFD implementation, including the physical models, meshing approach, porous-medium treatment, convergence procedure, and extracted quantities, as well as the experimental and simulation results, is provided in the Supplementary Information.

Given the large number of test specimens required, a time- and cost-efficient approach is essential for experimental data generation. To achieve this, the following methods are applied:

- **Experimental operation with inert gas and realistic flow conditions**
  Nitrogen is employed as the feed gas to ensure safe and inert operation instead of using real methanol synthesis syngases such as hydrogen, carbon monoxide, and carbon dioxide. To allow the experimental data to be applicable to different reactions and operating conditions, the fluid regime under real reaction conditions is replicated by adjusting the nitrogen flow rate. Therefore, the experiments are conducted with nitrogen flow rates ranging from 100 mL_n/min to 2000 mL_n/min, selected to match the Reynolds numbers observed in actual processes. Within the proposed framework, syngas flow rates are translated into equivalent nitrogen flow rates by equating the packed-bed Reynolds numbers. In a packed-bed, the flow regime is characterized by the packed-bed Reynolds number [56]

$$Re_{pb} = \frac{\rho v d_p}{\mu \cdot \epsilon}, \tag{3}$$

where ρ is the fluid density, v is the superficial velocity, μ is the dynamic viscosity, d_p is the effective particle diameter, and ϵ is the bed porosity. To ensure comparable flow behavior between the experimental system using nitrogen and the real system using syngas, the particle diameter d_p is fixed in the range of 0.1–0.2 mm, and the bed porosity ϵ is set to 0.4 in both applications. Under these conditions, the Reynolds numbers of both gases are equated as:

$$Re_{\mathrm{syn}} = Re_{\mathrm{N_2}} = \frac{\rho_{\mathrm{syn}} v_{\mathrm{syn}} d_p}{\mu_{\mathrm{syn}}(1-\epsilon)} = \frac{\rho_{\mathrm{N_2}} v_{\mathrm{N_2}} d_p}{\mu_{\mathrm{N_2}}(1-\epsilon)}. \tag{4}$$

The calculation of the Reynolds number requires accurate values for the dynamic viscosity μ, which strongly depends on temperature. To account for this temperature dependence, the dynamic viscosity of each gas is determined using Sutherland's law [57]:

$$\mu_i = \mu_{\mathrm{ref}} \left(\frac{T}{T_{\mathrm{ref}}}\right)^{3/2} \frac{T_{\mathrm{ref}} + S}{T + S}, \tag{5}$$

where μ_{ref} is the reference dynamic viscosity at the temperature T_{ref}, and S is the Sutherland constant characteristic of the gas. Once the viscosities of syngas and nitrogen are defined for the operating conditions, the nitrogen flow rate is calculated from Eq. (4). Since d_p and ϵ are identical in both applications, these terms cancel when solving the equality for the nitrogen flow rate:

$$\dot{V}_{\mathrm{N_2}} = \left(\frac{\mu_{\mathrm{N_2}}}{\mu_{\mathrm{syn}}}\right)\left(\frac{\rho_{\mathrm{syn}}}{\rho_{\mathrm{N_2}}}\right)\dot{V}_{\mathrm{syn}}. \tag{6}$$

Table 1
Investigated channel geometries and parameter ranges used for data generation.

Geometry	Dimension (mm)	Fixed relation	Length (mm)	Nitrogen flow rate ($mL_n\ min^{-1}$)
Round	3–15	–	50–100	100–2000
Rectangular	1.5–7.7	Aspect ratio = 1.5	50–100	100–2000
Helical	3–6	Fixed helical path	66.5	100–2000

This relation enables direct determination of the nitrogen flow rate required to reproduce the Reynolds number of syngas, ensuring that the same flow regime is achieved under experimental conditions.

- **Using specimen manufactured by vat-based photopolymerization with ultraviolet light (VPP-UVL/P)**
  AM reduces supply chain lead times compared to conventional fabrication methods and enables rapid testing. Metal AM, however, is costly when a large number of specimens is required. Therefore, VPP-UVL/P is used as a relatively inexpensive and time-efficient manufacturing approach in this study. While polymer materials cannot withstand high temperatures and pressures typical of real operating conditions, this limitation does not affect the experiments, as they are designed solely for geometric comparisons. The suitability of polymer specimens for geometric comparison of generated variants within the proposed framework can be justified analytically using the overall heat transfer coefficient, expressed as a series of thermal resistances according to standard heat-transfer design formulations [56]:

$$\kappa_j = \left(\frac{1}{\alpha_{i,j}} + \frac{\delta}{\lambda_w} + \frac{1}{\alpha_o} \right)^{-1}, \tag{7}$$

  where $\alpha_{i,j}$ denotes the inner convective heat-transfer coefficient of geometrical variant j, δ and λ_w are the wall thickness and thermal conductivity of the channel material, and α_o is the outer convective heat transfer coefficient.
  Within this study, the outer convective heat transfer coefficient can be assumed identical for all cases, as the mass flow rate of the thermal oil is maintained at 1.0 g s^{-1} in both the physical characteristic experiments and the reaction scenario. Additionally, the flow regime inside the channel is preserved by reproducing the same Reynolds number for the syngas under experimental conditions. Consequently, differences between metal and polymer configurations affect only the wall resistance term δ/λ_w, allowing the heat transfer coefficient to be consistently recalculated without altering the relative comparison of geometrical variants.

Additionally, the channels of the specimens are filled with an γ-Al_2O_3 industrial catalyst to capture the actual effects of packed-bed conditions (see Fig. 3). Due to the identical particle size range and bed porosity, the powder bed provides comparable packing conditions for evaluating geometry-dependent effects, as packed-bed heat transport is strongly influenced by particle size, porosity, and packing structure [58]. In the specimen design, two design parameters shown in Fig. 3, channel dimension and channel length, are varied for the experiments. The thermal oil connections are implemented using *Swagelok* 6 mm fittings with standard metal ferrules, while the packed-bed zone is connected through G1/8 interfaces to the test bench. Across the different test series, the channel geometry type is also changed, while all other specimen details remain unchanged. To summarize the investigated design space for data generation, Table 1 lists these design parameters together with the applied nitrogen flow rate range.

The parameter ranges in Table 1 are selected based on the considered methanol synthesis application and the experimental constraints of the test setup. For the round and rectangular channels, the selected dimensions cover the relevant channel dimension range for the investigated methanol synthesis cases. For the helical channels, the maximum channel diameter is limited to 6 mm, since larger diameters cannot be realized within the selected specimen length. The channel lengths are varied between 50 and 100 mm, while longer channels are not investigated because the associated increase in pressure drop could exceed the allowable operating pressure of the polymer test specimens. For the helical geometry, an axial length of 66.5 mm is selected, which corresponds to a 100 mm helical flow path. The nitrogen flow rate range is selected to cover the relevant application range used in the experimental study.

3.1.1. Heat transfer & radial temperature difference tests

Heat transfer experiments are carried out with nitrogen at ambient temperature and pressure as the process gas, while a thermal oil serves as the heating medium. The thermal oil temperature is set to 60 °C, which is the upper limit for the temperature resistance of the used manufacturing polymer resin *Formlabs V4 Clear*. To reduce heat losses to the surroundings, the test system is insulated with rockwool- and fiberglass-based thermal insulation during the experiments. As illustrated in Fig. 4, four type-K thermocouples provided by *Conatex* are installed at the gas and oil inlets and outlets. The heat transfer rate Q is determined from the gas-side measurements

$$Q = \dot{m}_{N_2}\, c_{p,N_2}\, \Delta T, \tag{8}$$

where $\dot{m}_{N_2}$ is the nitrogen mass flow rate, c_{p,N_2} the specific heat capacity of nitrogen, and ΔT the measured temperature rise between thermocouple 1 and 2, as illustrated in Fig. 4. The corresponding heat transfer coefficient κ follows from

$$\kappa = \frac{Q}{A_{lat}\, \Delta T_{lm}} \tag{9}$$

with A_{lat} the lateral heat exchange area and ΔT_{lm} the logarithmic mean temperature difference,

$$\Delta T_{lm} = \frac{\Delta T_1 - \Delta T_2}{\ln\left(\Delta T_1 / \Delta T_2\right)}, \tag{10}$$

where ΔT_1 and ΔT_2 denote the inlet-to-outlet temperature differences of nitrogen and thermal oil, respectively [56]. The resulting κ values serve both as training data for the surrogate models and as reference data for validating the CFD simulation for heat transfer model. Radial temperature differences cannot be captured experimentally with sufficient accuracy, and are therefore obtained exclusively from the CFD results. The temperature values are extracted at the outlet planes of the individual channels. For each geometry, the maximum and minimum outlet temperatures among the channels are identified and their difference is calculated.

3.1.2. Pressure drop & flow profile

Pressure drop experiments are performed with nitrogen at ambient conditions as the working fluid. To protect the pressure transmitter and maintain safe operation, the same particle filters are installed both upstream and downstream of each specimen for all measurements (see Fig. 4). A single *WIKA S-20* transmitter records the inlet pressure, while the downstream side is open to the atmosphere after Filter 2, providing an ambient reference. The ambient pressure in the laboratory is monitored using a laboratory barometer and used as the outlet reference. The differential pressure is evaluated as

$$\Delta p = p_{inlet} - p_{ambient}. \tag{11}$$

These measurements supply the training data for the surrogate model that predicts pressure drop and serve as reference values for validating the CFD flow model. CFD simulations complement the experimental pressure drop data by providing velocity profiles for each geometry at the upper and lower limits of the particle-diameter tolerance band. For each variant, the two simulations are averaged to reflect the practical tolerance in particle diameter during experiments. The used catalyst powder are classified with laboratory sieves rather than

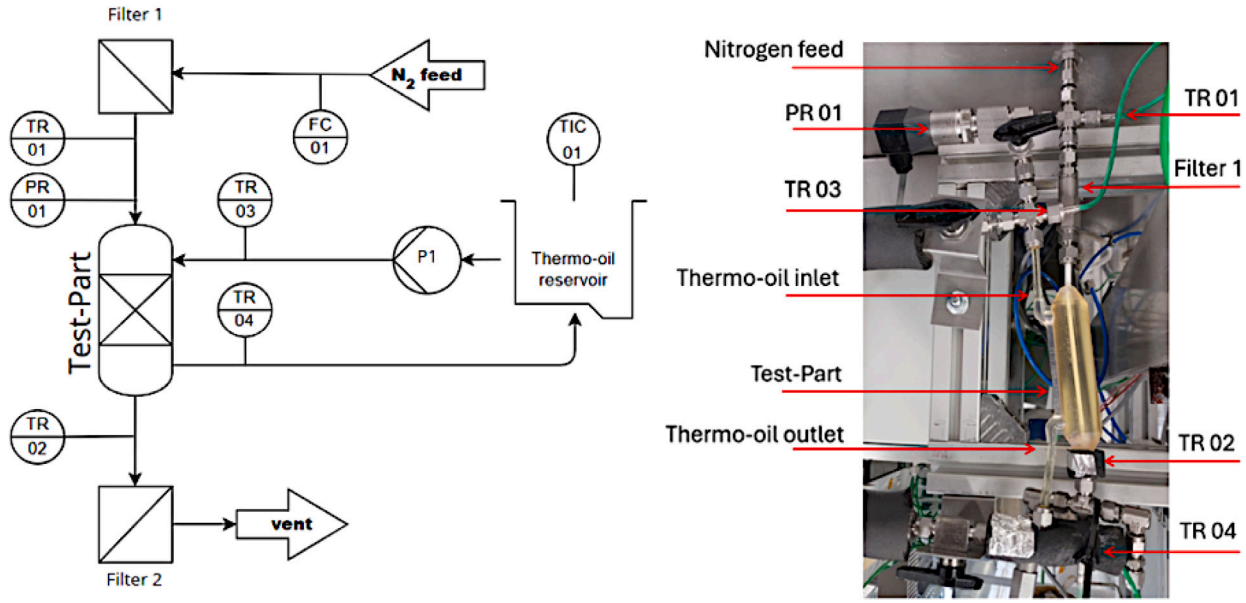

Fig. 4. Experimental setup for heat transfer and pressure drop tests with thermocouples (TR), pressure transmitter (PR), flow controller (FC), and pump (P1).

Table 2
Data sources used for training the surrogate models.

Physical characteristic	Training data source
Heat-transfer coefficient, κ	Experimental and CFD simulation data
Radial temperature difference	CFD simulation data
Pressure difference	Experimental data
Axial velocity difference	CFD simulation data

Table 3
Performance metrics of the surrogate models.

Surrogate model	R^2	RMSE	
Heat Transfer	0.8218	11.9986	$W\,m^{-1}\,K^{-1}$
Radial Temperature Difference	0.8199	0.2228	K
F Pressure Drop	0.8980	0.2129	bar
Flow Profile	0.8176	0.0164	$m\,s^{-1}$

manufactured to a single size, yielding a sieve cut that spans roughly 0.10–0.20 mm. Within this range, even small deviations in d_p affect both pressure loss and flow distribution; averaging the simulations at the lower and upper diameter limits therefore provides a representative reference value. The axial velocity values are extracted at the outlet planes of the individual channels. For each particle-diameter case, the maximum and minimum outlet axial velocities among the channels are identified and their difference is calculated. This difference is then averaged over the lower and upper particle-diameter limits to obtain the final value for each geometry.

3.2. Prediction of physical characteristics

Based on the collected experimental and simulation data, four surrogate models are developed, one each for heat transfer, radial temperature difference, pressure drop, and flow profile, to predict the physical characteristics defined in Section 3.1 for every channel geometry candidate. Table 2 summarizes the data source used for training each surrogate model. The complete dataset, including experimental measurements and CFD simulation results, is provided in the Supplementary Material.

Predicting these physical characteristics constitutes a supervised regression task. Among the ML algorithms evaluated in Section 2.3, including random forest regressors, artificial neural networks, support-vector regression, and gradient-boosting machines, the random-forest regressor demonstrated the highest predictive fidelity using *sckit-learn* library of *Python* programming language. Random forest algorithms use decision trees and they can deal with tabular datasets [59,60]. The datasets in this study consist of clearly defined input features (e.g., geometry type, inlet volumetric flow rate, channel dimension, channel length and inlet temperatures) and corresponding output variables (e.g., kappa value, temperature difference, pressure difference, and maximum axial velocity difference), which makes random forests a suitable choice for surrogate modeling. Additionally, the surrogate models in the proposed framework require training only once prior to deployment, which makes the computational cost of model training negligible.

Hyperparameter tuning uses grid search, which trains and evaluates the model for every combination of parameters in a predefined grid, using cross-validation to identify the configuration that yields the highest performance [61]. In this study, the tuning process explores the number of trees, maximum tree depth, minimum samples per leaf, and the fraction of features considered at each split, while keeping the random state fixed to ensure reproducibility. The training follows an 80/20 train–test split, where only the training set is used during the tuning phase. Each parameter combination is evaluated through five-fold cross-validation, where the training set is divided into five equal parts, the model trains on four parts, and validates on the remaining part in rotation [62]. The final hyperparameters selected by grid search for the four random forest surrogate models are summarized in the Supplementary Information. The implementation scripts for the surrogate models are publicly accessible through a GitHub repository [63].

The reliability of these models is quantified with the coefficient of determination R^2 and the RMSE, defined in Eqs. (1) and (2). Table 3 summarizes the calculated R^2 and RMSE for each surrogate model, demonstrating that all models achieve strong predictive performance across the evaluated physical characteristics.

The surrogate models developed in this work show consistent performance across the considered target variables. The reported R^2 and RMSE values are calculated on the hold-out test set. For the heat transfer model, the R^2 is 0.8218, indicating that approximately 82% of the variance in the test data is captured, with an RMSE of 11.9986 $W\,m^{-1}\,K^{-1}$. The comparatively larger error in absolute terms reflects the broader value range of the heat transfer coefficient and

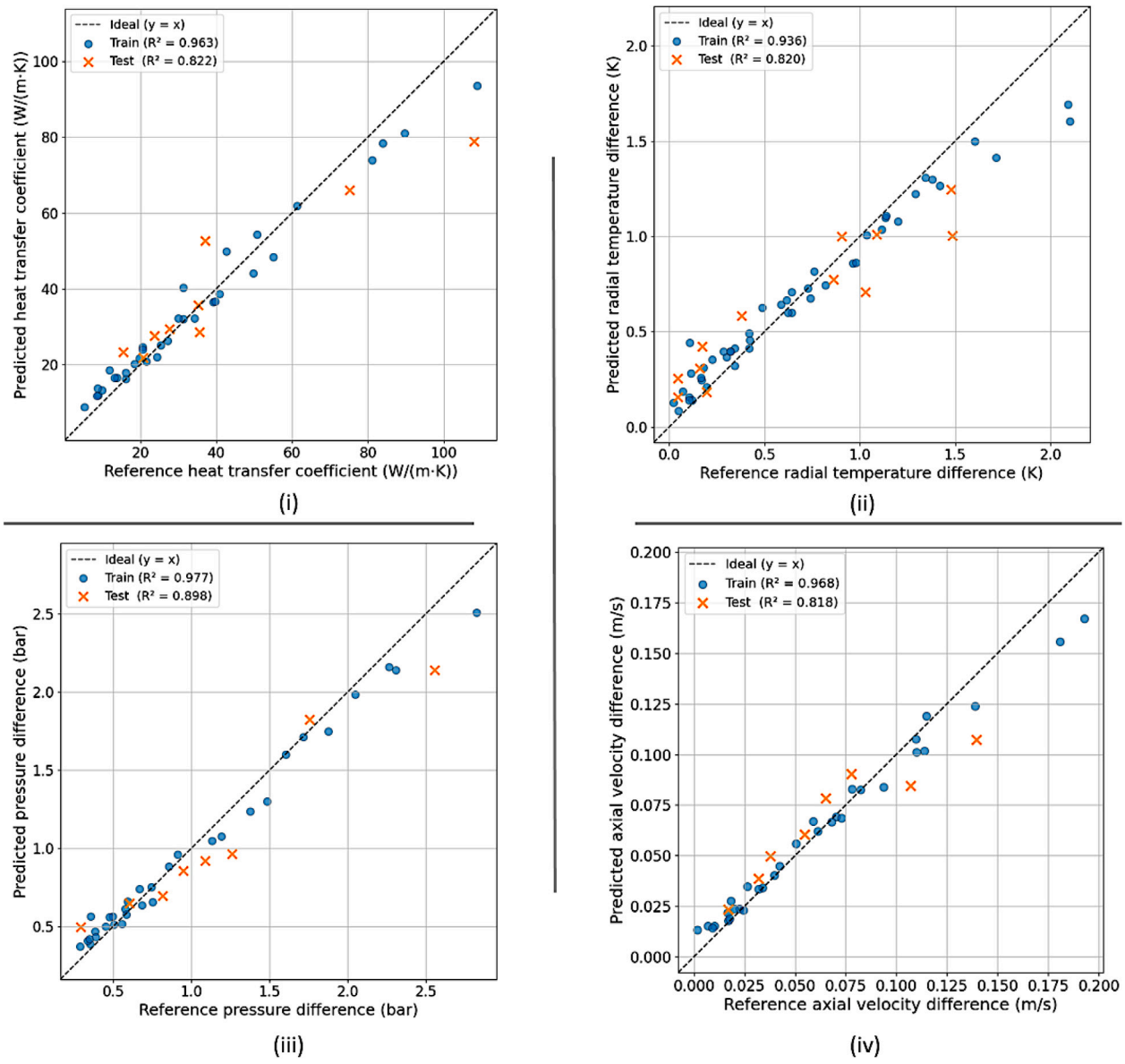

Fig. 5. Parity plots of surrogate model predictions versus reference values for: (i) heat transfer coefficient, (ii) radial temperature difference, (iii) pressure difference, (iv) axial velocity difference.

the different uncertainty sources associated with the experimental and CFD simulation data used for this surrogate model (see Table 2). The radial temperature difference model achieves an R^2 of 0.8199 and an RMSE of 0.2228 K, providing sufficient accuracy for assessing thermal homogeneity across channel configurations. The pressure drop model attains an R^2 of 0.8980 with an RMSE of 0.2129 bar, while the axial velocity difference model reaches an R^2 of 0.8176 and an RMSE of 0.0164 m s^{-1}. The parity plots in Fig. 5 show that the predictions follow the ideal one-to-one line across most of the investigated value range for all four surrogate models. Slightly larger deviations are observed near the upper end of some output ranges, where fewer reference samples are available. The corresponding residual plots are provided in the Supplementary Information. Taken together, these results show that the surrogate models capture the main trends of the data with sufficient accuracy for early-stage reactor channel geometry selection.

3.3. Decision making of reactor channel geometry selection

In the proposed framework, the reactor channel geometry is selected using the TOPSIS method, a MCDM approach chosen from the methods described in Section 2.2, to rank the generated channel variants based on predefined criteria and identify the most suitable parameter configurations. TOPSIS is employed because it offers a transparent procedure and provides a clear ranking of alternatives according to their proximity to the ideal solution. The calculation details of the TOPSIS ranking procedure are provided in the Supplementary Material, following the standard TOPSIS formulation [37,38]. The criteria are defined to address two primary objectives: maximizing reactor performance and minimizing manufacturing costs through compact reactor design. The selection process starts after defining the reactor volume, which is obtained from an analytical PFR calculation for a reference multitubular reactor model (see Fig. 2). Based on this volume, all possible channel variants of geometry data are generated to establish the solution space. For the generation process, a step size of 0.1 mm is applied to the channel dimensions to enhance the sensitivity of the decision making framework, improve the resolution for identifying suitable variants, and provide sufficient data for training ML models. The flow rates of nitrogen are then calculated using Eqs. (3)–(6), and these equivalent nitrogen flows are employed in the surrogate models to predict the

Table 4
Rule-based filtering constraints.

Constraint	Threshold
Radial temperature difference	$\leq 0.5\,\mathrm{K}$
Pressure drop	$\leq 1.0\,\mathrm{bar}$
Axial velocity difference	$\leq 0.08\,\mathrm{m/s}$

Table 5
TOPSIS ranking weights.

Criterion	Weight
Heat transfer coefficient, κ	0.3
Pressure drop	0.1
Channel length	0.6

corresponding physical characteristics. This step is followed by a rule-based filtering procedure to eliminate non-viable configurations. The rule-based filtering step applies the following constraints (see Table 4).

Only configurations that satisfy all predefined requirements are retained for further evaluation. This filtering process ensures the prevention of hot-spot formation and maintains adequate pressure control. To avoid hot-spot formation in exothermic reactors and to sustain near-isothermal operation, effective control of both radial and axial heat transfer is essential [25]. For this purpose, we apply a rule that limits the radial temperature difference to $\leq 0.5,\mathrm{K}$ and define the overall heat transfer conductivity, κ, is used as the selection criterion for heat transfer performance, as defined in Section 3.1.1. Additional rules, such as pressure drop and axial velocity difference, ensure optimal conditions for methanol synthesis. After this filtering step, the ranking process emphasizes the overarching objective of compact reactor design while still accounting for thermal performance and operability. To reflect these priorities, the channel length receives the highest weight (0.6), since shorter channels directly translate into a more compact reactor volume and lower manufacturing costs. Heat transfer receives a moderate weight (0.3) to ensure sufficient thermal management, which is critical for methanol synthesis. Pressure drop receives the lowest weight (0.1), as it is less critical under the considered operating conditions, yet remains relevant for operability and energy efficiency. The remaining variants are subsequently ranked using the TOPSIS method, based on these weighted criteria, which Table 5 summarizes.

The highest-scoring variants are provided to the reactor designer as recommendations. Rather than pursuing full automation, the framework is designed to support the decision making process, as the designer's expertise remains essential for evaluating practical considerations beyond the defined criteria. The tool thus serves as decision support, while the final selection is made by the reactor designer. The implementation script of decision making structure is publicly accessible through a GitHub repository [63].

4. Results & discussion

The evaluation of the proposed framework is carried out along two dimensions: (i) achieving the desired reaction conditions using the framework without the need for additional reaction tests and (ii) demonstrating its advantages across different application scenarios. Both evaluations are performed with an experimentally validated CFD simulation of methanol synthesis. To isolate the framework assessment from the influence of the cooling fluid profile in the whole reactor and to avoid the need for optimization of the overall reactor design, including manifolding, syngas distribution, thermal oil routing and manufacturing related aspects, the channel variants are simulated under reaction conditions while maintaining the same geometrical designs as those used in the experimental heat transfer tests described in Section 3.1. The validation procedure for this CFD model is described in detail in our previous work [23].

4.1. Achieving desired reaction conditions with the proposed framework

As highlighted in Section 2.1, precise control of pressure and temperature is essential in the design of methanol synthesis reactors. To ensure optimal reaction conditions, the reactor temperature profile should remain as close as possible to isothermal. Since the literature does not provide a universally accepted definition of near-isothermal operation, we define it here as a maximum temperature deviation of less than 2 K. This criterion is consistent with the maximum temperature difference associated with the kinetic model adopted from the literature and applied in our CFD simulations [51]. Since the nitrogen flow rates are adjusted to match the packed-bed Reynolds numbers of the corresponding syngas cases, the simplified experimental setup described in Section 3.1.2 is used to approximate the packed-bed behavior relevant to the methanol synthesis reactor. Consequently, the rule-based limits derived from these experiments can also be applied as practical thresholds for defining the optimal operating conditions in methanol synthesis.

To demonstrate the achievement of these conditions within a compact reactor design, we implement a representative case study using the proposed framework. The input parameters are defined as follows:

- Target methanol yield: 100 L/day
- Flange dimension: 350 mm × 350 mm
- Inlet cooling flow rate: 1 g/s

As described in Fig. 2, the framework first executes the PFR model. This model analytically determines the reactor volume required to achieve the target methanol yield and calculates the corresponding channel length based on the given channel and flange dimensions. The number of channels and their length are derived using the spacing algorithm integrated into the model, which is described in the Supplementary Material and implemented in the PFR model available on GitHub [54]. Using these reference channel dimensions, the MCDM process is then conducted automatically to identify all variants that satisfy the optimal operating conditions for methanol synthesis. The identified variants are subsequently ranked according to the procedure explained in Section 3, with the final ranking performed using user-defined weights in TOPSIS. In this case study, the high target methanol production rate of 100 L/day leads to a considerable heat release from the reaction, which increases the importance of efficient heat removal. Accordingly, the framework predominantly suggests rectangular channel variants, which is reasonable given the spacing advantages of rectangular geometries in applications that require high heat removal. Finally, the reference channel, together with the best-performing rectangular and round variants, is simulated using the methanol synthesis reaction model to verify whether the defined optimal operating conditions are achieved (see Table 6).

Table 6 summarizes the key operating parameters of the evaluated variants. The reported channel counts represent sizing results for the given input parameters, not finalized manifolded reactor layouts. Practical implementation requires subsequent deterministic reactor design, including manifold design, syngas distribution, thermal oil routing and manufacturing related aspects. The reference round channel shows a temperature rise of about 4 K, which exceeds the defined near-isothermal criterion and therefore does not meet the required operating conditions. By contrast, the best rectangular and round variants remain within the acceptable limits, while the observed increases in pressure drop and axial flow difference are still below the defined thresholds.

Fig. 6 illustrates the corresponding temperature distributions. In the reference channel, a pronounced hot spot develops near the inlet due to the higher syngas concentration and consequently higher reaction rate at this location. For the best rectangular and round variants, the maximum deviations remain below 2 K, with only localized inlet hot spots observed. Overall, both optimized variants exhibit a stable axial temperature profile without significant gradients along the channel

Table 6
Comparison of the reference and optimal variants suggested by the framework (Case 1).

Variant	Geometry type	Dim. (mm)	Length (mm)	Number of channels	T_{in} (K)	T_{max} (K)	Δp (bar)	Flow Diff. (m/s)	TOPSIS (%)
Reference Variant	Round	15	62.00	247	525	529.2	0.0127	0.0029	Filtered
Variant 1	Rectangular	5–3	86.60	1866	525	526.4	0.0253	0.0062	57.9
Variant 2	Round	4.68	99.99	1570	525	526.6	0.0357	0.0070	49.8

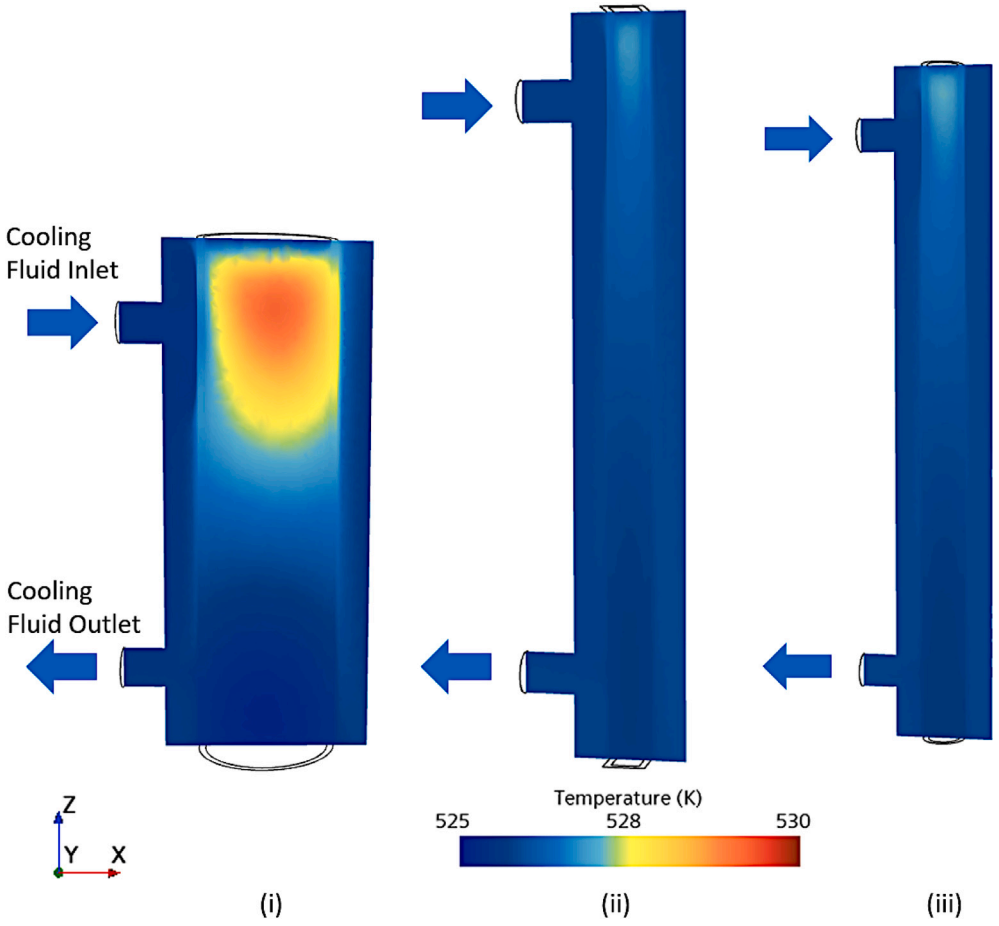

Fig. 6. Temperature Profiles for case study 1: (i) Reference variant, (ii) Variant 1, (iii) Variant 2.

length. These results demonstrate that the proposed framework distinguishes between geometries that exceed the thermal limits and those capable of maintaining near-isothermal operation. Detailed results of this test are provided in the Supplementary Information.

4.2. Demonstrating of the proposed framework in different applications

To further evaluate the proposed framework under different requirements, an additional representative case study is carried out. In this scenario, the input parameters are selected to optimize the channel variants for a small-scale reactor application. The parameters are defined as follows:

- Target methanol yield: 1 L/day
- Flange dimension: 120 mm × 120 mm
- Inlet cooling flow rate: 1 g/s

With this configuration, the proposed framework is executed, and the best-ranked variants are identified as described in Section 4.1. In contrast to the first case study, the framework here tends to favor round channel variants (see Table 7). This outcome is mainly attributed to the shorter channel lengths offered by round geometries, which received the highest weight in the evaluation process. The underlying reason for this tendency is less radial temperature difference and the higher achievable κ values in the corresponding flow regime. The flow regime itself is determined by the volumetric flow rate per channel, which is influenced by parameters such as the target methanol yield, channel dimensions, and flange size. As the resulting temperature profiles are comparable to those in the first case study, they are not presented separately here.

In both representative case studies, round and rectangular channels remained viable reactor geometries, whereas helical variants generally achieved higher κ values (see Supplementary Information). However, the number of helical channels that can be accommodated within the defined flange size is markedly lower than for the other geometries. Consequently, helical designs require substantially longer channel lengths, which increase pressure drop and conflict with the evaluation criterion on channel length. Even so, reactors with helical channels can be advantageous for strongly exothermic reactions or serve as qualitative benchmarks for alternative concepts. Overall, the case studies illustrate the framework's versatility in addressing diverse reactor design requirements.

Table 7
Comparison of the reference and optimal variants suggested by the framework (Case 2).

Variant	Geometry type	Diam. (mm)	Length (mm)	Number of channels	T_{in} (K)	T_{max} (K)	Δp (bar)	Flow (m/s)	TOPSIS (%)
Reference Variant	Round	15	73.00	2	520	525.86	0.0263	0.0054	Filtered
Variant 1	Round	4.08	50.5	39	520	521.053	0.0109	0.0052	94.9
Variant 2	Rectangular	4–3	52.83	33	520	521.117	0.01143	0.0056	89.5

4.3. Limitations & further developments

The proposed framework supports the early-stage selection of reactor channel geometries by enabling reactor designers to identify suitable channel geometry and its parameter configurations without additional experimental or numerical studies for each channel geometry. In our previous work [23], we highlighted the necessity of a probabilistic preselection step for reactor channels as part of an automated design workflow. Building on this, the present framework addresses that need and reduces computational effort by providing data-driven guidance for geometry selection at an early stage.

The underlying methodology is designed for broad applicability because it relies on physical characteristics instead of reaction-specific results. These parameters represent fundamental properties of channel configurations and remain valid across different chemical reactions. In addition, the framework provides a basis for incorporating further geometries, including more complex configurations, into the selection process as long as their physical characteristics can be defined. Such geometries can be integrated into the framework using validated CFD simulations of the physical characteristics or through additional experimental studies following the procedure described in Section 3.1. The framework can also be extended by integrating further physical aspects, such as fouling, thereby broadening the scope of the decision making process. Nevertheless, the relative importance of these characteristics may vary depending on the application, which implies that the weighting scheme within the decision making process needs to be adapted to the specific process requirements.

Despite its advantages, the proposed framework has certain limitations. The definition of appropriate weights is reaction-specific, and inaccurate weighting can bias the ranking of candidate geometries. Similarly, the rules applied in the filtering stage need to be tailored to the requirements of each application. For this reason, the framework supports the reactor designer in the decision making process, but the final responsibility still lies with the engineer. Moreover, while the framework provides reliable early-stage guidance, it does not replace the subsequent deterministic design stages, such as detailed CAD followed by CFD simulations and experimental validation, which remain essential to confirm and finalize the reactor design.

5. Conclusion

This work presents a data-driven framework for the early-stage selection of reactor channel geometries. By relying on fundamental physical characteristics, such as heat transfer, radial temperature difference, pressure drop and flow profile, rather than reaction-specific results, the framework enables the efficient identification of suitable channel geometry and its parameter configurations. The framework integrates surrogate models to predict key physical characteristics across a wide range of channel variants, and employs the TOPSIS multi-criteria decision making method to rank these variants against predefined objectives. In addition, the framework provides a first probabilistic dimensioning of reactor channels, which reduces the number of experimental and numerical investigations required during detailed optimization. The applicability of the framework is demonstrated through two case studies in methanol synthesis, highlighting its capability to support reactor designers in early-stage decision making. However, the framework is intended to support the reactor designer, while the final reactor design still requires application-specific weighting, rule definition, detailed CAD development, CFD simulations, and experimental validation. Beyond these applications, the methodology also establishes a foundation for incorporating more complex channel designs and extending the approach to other reaction systems, provided that the relevant physical characteristics can be described.

CRediT authorship contribution statement

Mertcan Kaya: Writing – original draft, Validation, Software, Methodology. **Jean-Luc Göttsche:** Validation, Data curation. **Christoph Klahn:** Writing – review & editing, Funding acquisition.

Declaration of Generative AI and AI-assisted technologies in the writing process

During the preparation of this work the authors used ChatGPT in order to improve the readability and the language of the manuscript. After using this tool, the authors reviewed and edited the content as needed and take full responsibility for the content of the published article.

Declaration of competing interest

The authors declare that they have no known competing financial interests or personal relationships that could have appeared to influence the work reported in this paper.

Acknowledgments

The authors thank Vignesh Jayavelu for his support in supervision of the students and Manuel Hofheinz for his support in manufacturing and post-processing of the test specimen.

This work is supported by the BMWE 3D-Process project (project no. 03EN2065E). 3D-Process is financed by Federal Ministry for Economic Affairs and Climate Protection from Germany.

Appendix A. Supplementary data

Supplementary material related to this article can be found online at https://doi.org/10.1016/j.cej.2026.178541.

Data availability

Research Link Provided

Supplement (Original data) (GitHub)
Supplementary Data (Original data) (Mendeley Data)

References

[1] O.A. Alimi, R. Meijboom, Current and future trends of additive manufacturing for chemistry applications: a review, J. Mater. Sci. 56 (30) (2021) 16824–16850, http://dx.doi.org/10.1007/s10853-021-06362-7.

[2] C. Parra-Cabrera, C. Achille, S. Kuhn, R. Ameloot, 3D printing in chemical engineering and catalytic technology: structured catalysts, mixers and reactors, Chem. Soc. Rev. 47 (1) (2018) 209–230, http://dx.doi.org/10.1039/c7cs00631d.

[3] A. Hauser, M. Neubert, A. Feldner, A. Horn, F. Grimm, J. Karl, Design and implementation of an additively manufactured reactor concept for the catalytic methanation, Appl. Sci. 12 (18) (2022) 9393, http://dx.doi.org/10.3390/app12189393.

[4] M.L. Schulte, V. Truttmann, D.E. Doronkin, L. Baumgarten, A. Nicolai, D.A. Montalvo Beltran, F.J. Summ, C. Kiener, L. Warmuth, S. Pitter, E. Saraçi, J.-D. Grunwaldt, Monitoring the fate of Zn in the Cu/ZnO/ZrO_2 catalyst during CO_2-to-methanol synthesis at high conversions by operando spectroscopy, Angew. Chem. Int. Ed. 64 (15) (2025) http://dx.doi.org/10.1002/anie.202423281.

[5] W. Hou, A. Bubliauskas, P.J. Kitson, J.-P. Francoia, H. Powell-Davies, J.M.P. Gutierrez, P. Frei, J.S. Manzano, L. Cronin, Automatic generation of 3D-printed reactionware for chemical synthesis digitization using chemscad, Org. Chem. Front. 8 (5) (2021) 1060–1067, http://dx.doi.org/10.1039/D0QO01154A.

[6] D. Li, T. Maloney, N. Mannan, S.A. Niknam, Design of additively manufactured methanol conversion reactor for high throughput production, Mater. Des. Process. Commun. 3 (1) (2020) e143, http://dx.doi.org/10.1002/mdp2.143.

[7] T. Savage, N. Basha, J. McDonough, J. Krassowski, O.K. Matar, E.A. del Rio Chanona, Machine learning-assisted discovery of flow reactor designs, Nat. Chem. Eng. (2023) http://dx.doi.org/10.1038/s44286-024-00099-1.

[8] K.N. Otto, E.K. Antonsson, Trade-off strategies in engineering design, Res. Eng. Des. 3 (2) (1991) 87–103, http://dx.doi.org/10.1007/BF01581342.

[9] J.-W. Seo, Y.-H. Kim, D. Kim, Y.-D. Choi, K.-J. Lee, Heat transfer and pressure drop characteristics in straight microchannel of printed circuit heat exchangers, Entropy 17 (5) (2015) 3438–3457, http://dx.doi.org/10.3390/e17053438.

[10] VDI 2221 Part 1: Development of Technical Products and Systems – Model of Systematic Approach, 2019, VDI-Richtlinie 2221 Blatt 1.

[11] T. Shealy, J. Gero, M. Hu, J. Milovanovic, Concept generation techniques change patterns of brain activation during engineering design, Des. Sci. 6 (2020) 31–58, http://dx.doi.org/10.1017/dsj.2020.30.

[12] K. Miettinen, Nonlinear multiobjective optimization, in: International Series in Operations Research & Management Science, vol. 12, Kluwer Academic Publishers, Boston, 1999, http://dx.doi.org/10.1007/978-1-4615-5563-6.

[13] A. Mosavi, A multicriteria decision making environment for engineering design and production decision-making, Int. J. Comput. Appl. 69 (1) (2013) 26–38, http://dx.doi.org/10.5120/11807-7457.

[14] H. Kordabadi, A. Jahanmiri, Optimization of methanol synthesis reactor using genetic algorithms, Chem. Eng. J. 108 (3) (2005) 249–255, http://dx.doi.org/10.1016/j.cej.2005.02.023.

[15] Y.M. Goh, C.A. McMahon, J.D. Booker, Improved utility and application of probabilistic methods for reliable mechanical design, Proc. Inst. Mech. Eng. Part O: J. Risk Reliab. 223 (3) (2009) 199–214, http://dx.doi.org/10.1243/1748006XJRR244.

[16] G. Maglaras, E. Ponslet, R.T. Haftka, E. Nikolaidis, P. Sensharma, H.H. Cudney, Analytical and experimental comparison of probabilistic and deterministic optimization, AIAA J. 34 (7) (1996) 1512–1518, http://dx.doi.org/10.2514/3.13261.

[17] Institut für Technische Mechanik, KIT, Skript CVT-i version 2.4, 2024, Lecture Script, Karlsruhe Institute of Technology (KIT), https://www.itm.kit.edu.

[18] C. Hu, Reactor design and selection for effective continuous manufacturing of pharmaceuticals, J. Flow Chem. 11 (3) (2021) 243–263, http://dx.doi.org/10.1007/s41981-021-00164-3.

[19] A.K. Coker, Chapter 21 - industrial and laboratory reactors – chemical reaction hazards and process integration of reactors, in: A.K. Coker (Ed.), Ludwig's Applied Process Design for Chemical and Petrochemical Plants (Fourth Edition), Fourth Edition, Gulf Professional Publishing, Boston, 2015, pp. 1095–1208, http://dx.doi.org/10.1016/B978-0-08-094242-1.00021-8.

[20] E. Magnanelli, S.B.B. Solberg, S. Kjelstrup, Nature-inspired geometrical design of a chemical reactor, Chem. Eng. Res. Des. 152 (2019) 20–29, http://dx.doi.org/10.1016/j.cherd.2019.09.022.

[21] J. Cho, J. Marquis, P. Trogadas, T. Neville, D. Brett, M.-O. Coppens, Optimizing the architecture of lung-inspired fuel cells, Chem. Eng. Sci. 215 (2020) 115375, http://dx.doi.org/10.1016/j.ces.2019.115375.

[22] M. Kaya, C. Klahn, Sequential parameter optimization for algorithm-based design generation using data from multiphysics simulations, Procedia CIRP 119 (2023) 1234–1239, http://dx.doi.org/10.1016/j.procir.2023.02.191, The 33rd CIRP Design Conference.

[23] M. Kaya, C. Klahn, Automated design of additively manufactured reactors for decentralized methanol production, 2026, http://dx.doi.org/10.2139/ssrn.6156316.

[24] B. Dash, J. Nanda, S.K. Rout, The role of microchannel geometry selection on heat transfer enhancement in heat sinks: A review, Heat Transf. 51 (2) (2022) 1406–1424, http://dx.doi.org/10.1002/htj.22357.

[25] V. Dieterich, A. Buttler, A. Hanel, H. Spliethoff, S. Fendt, Power-to-Liquid via synthesis of Methanol, DME or Fischer–Tropsch-Fuels: a review, Energy & Environ. Sci. 13 (10) (2020) 3207–3252, http://dx.doi.org/10.1039/D0EE01187H.

[26] M. Ebrahimzadeh Sarvestani, O. Norouzi, F. Di Maria, A. Dutta, From catalyst development to reactor design: A comprehensive review of methanol synthesis techniques, Energy Convers. Manage. 302 (2024) 118070, http://dx.doi.org/10.1016/j.enconman.2024.118070.

[27] M. Son, Y. Woo, G. Kwak, Y.-J. Lee, M.-J. Park, CFD modeling of a compact reactor for methanol synthesis: Maximizing productivity with increased thermal controllability, Int. J. Heat Mass Transfer 145 (2019) 118776, http://dx.doi.org/10.1016/j.ijheatmasstransfer.2019.118776.

[28] M.R. Rahimpour, M. Lotfinejad, Enhancement of methanol production in a membrane dual-type reactor, Chem. Eng. Technol. 30 (8) (2007) 1062–1076, http://dx.doi.org/10.1002/ceat.200700114.

[29] S.S. Iyer, T. Renganathan, S. Pushpavanam, M. Vasudeva Kumar, N. Kaisare, Generalized thermodynamic analysis of methanol synthesis: Effect of feed composition, J. CO_2 Util. 10 (2015) 95–104, http://dx.doi.org/10.1016/j.jcou.2015.01.006.

[30] R. Krishna, S. Sie, Strategies for multiphase reactor selection, Chem. Eng. Sci. 49 (24, Part A) (1994) 4029–4065, http://dx.doi.org/10.1016/S0009-2509(05)80005-3, Chemical Reaction Engineering: Science & Technology.

[31] S. Haase, C.A. de Araujo Filho, J. Wärn˚ a, D.Y. Murzin, T. Salmi, Reactor selection for upgrading hemicelluloses: Conventional and miniaturised reactors for hydrogenations, Processes 9 (9) (2021) http://dx.doi.org/10.3390/pr9091558.

[32] Z. Wang, S.R. Nabavi, G.P. Rangaiah, Multi-criteria decision making in chemical and process engineering: Methods, progress, and potential, Processes 12 (11) (2024) http://dx.doi.org/10.3390/pr12112532.

[33] S. Malefaki, D. Markatos, A. Filippatos, S. Pantelakis, A comparative analysis of multi-criteria decision-making methods and normalization techniques in holistic sustainability assessment for engineering applications, Aerospace 12 (2) (2025) http://dx.doi.org/10.3390/aerospace12020100.

[34] S. Greco, M. Ehrgott, J.R. Figueira, Multiple criteria decision analysis: State of the art surveys, 2nd ed., in: International Series in Operations Research & Management Science, vol. 233, Springer, New York, 2016, http://dx.doi.org/10.1007/978-1-4939-3094-4.

[35] H. Taherdoost, M. Madanchian, Multi-criteria decision making (MCDM) methods and concepts, Encyclopedia 3 (2023) 77–87, http://dx.doi.org/10.3390/encyclopedia3010006.

[36] M. Aruldoss, T.M. Lakshmi, V.P. Venkatesan, A survey on multi criteria decision making methods and its applications, Am. J. Inf. Syst. 1 (1) (2013) 31–43, http://dx.doi.org/10.12691/ajis-1-1-5.

[37] J.J. Thakkar, Multi-criteria decision making, in: Studies in Systems, Decision and Control, vol. 336, Springer, Cham, 2021, http://dx.doi.org/10.1007/978-3-030-77465-6.

[38] M. Yazdani, A. Farokh Payam, A comparative study on material selection of microelectromechanical systems electrostatic actuators using ashby, VIKOR and TOPSIS, Mater. Des. 65 (2015) 328–334, http://dx.doi.org/10.1016/j.matdes.2014.09.004.

[39] L. Xiaomin, H. Shuiping, C. Yuting, Research and application: conceptual integrated model based on TRIZ and bionics for product innovation, Int. J. Interact. Des. Manuf. (IJIDeM) 11 (2) (2017) 341–349, http://dx.doi.org/10.1007/s12008-015-0296-x.

[40] M. Youssef, B. Webster, A multi-criteria decision making approach to the new product development process in industry, Rep. Mech. Eng. 3 (1) (2022) 83–93, http://dx.doi.org/10.31181/rme2001260122y.

[41] S.R. Nabavi, Z. Wang, M.L. Rodríguez, Multi-objective optimization and multi-criteria decision-making approach to design a multi-tubular packed-bed membrane reactor in oxidative dehydrogenation of ethane, Energy & Fuels 39 (1) (2025) 491–503, http://dx.doi.org/10.1021/acs.energyfuels.4c03101.

[42] A. Papadopoulos, A. Karagiannidis, Application of the multi-criteria analysis method Electre III for the optimisation of decentralised energy systems, Omega 36 (5) (2008) 766–776, http://dx.doi.org/10.1016/j.omega.2006.01.004.

[43] Z. Wang, J. Li, G.P. Rangaiah, Z. Wu, Machine learning aided multi-objective optimization and multi-criteria decision making: Framework and two applications in chemical engineering, Comput. Chem. Eng. 165 (2022) 107945, http://dx.doi.org/10.1016/j.compchemeng.2022.107945.

[44] S.R. Nabavi, M.J. Jafari, Z. Wang, Deep learning aided multi-objective optimization and multi-criteria decision making in thermal cracking process for olefines production, J. the Taiwan Inst. Chem. Eng. 152 (2023) 105179, http://dx.doi.org/10.1016/j.jtice.2023.105179.

[45] S.R. Nabavi, Z. Guo, Z. Wang, Machine learning-assisted surrogate modeling with multi-objective optimization and decision-making of a steam methane reforming reactor, 2025, http://dx.doi.org/10.48550/arXiv.2507.07641.

[46] Z. Zhang, D. Zhang, M. Zhu, H. Zhao, X. Zhou, H. Yan, C. Yang, Machine learning assisted reactor and full process optimization design for alcohol oxidation, Chem. Eng. Sci. 305 (2025) 121165, http://dx.doi.org/10.1016/j.ces.2024.121165.

[47] Z. Wang, W.G.Y. Tan, G.P. Rangaiah, Z. Wu, Machine learning aided model predictive control with multi-objective optimization and multi-criteria decision making, Comput. Chem. Eng. 179 (2023) 108414, http://dx.doi.org/10.1016/j.compchemeng.2023.108414.

[48] A. Géron, Hands-On Machine Learning with Scikit-Learn, Keras, and TensorFlow, second ed., O'Reilly Media, Sebastopol, CA, 2019.
[49] T. Chai, R.R. Draxler, Root mean square error (RMSE) or mean absolute error (MAE)? – arguments against avoiding RMSE in the literature, Geosci. Model. Dev. 7 (3) (2014) 1247–1250, http://dx.doi.org/10.5194/gmd-7-1247-2014.
[50] D. Chicco, M. Warrens, G. Jurman, The coefficient of determination R-squared is more informative than SMAPE, MAE, MAPE, MSE and RMSE in regression analysis evaluation, PeerJ Comput. Sci. 7 (2021) e623, http://dx.doi.org/10.7717/peerj-cs.623.
[51] B.L.d. Campos, K.H. Delgado, S. Wild, F. Studt, S. Pitter, J. Sauer, Surface reaction kinetics of the methanol synthesis and the water gas shift reaction on $Cu/ZnO/Al_2O_3$, React. Chem. Eng. 6 (5) (2021) 868–887, http://dx.doi.org/10.1039/D1RE00040C.
[52] H.S. Fogler, Elements of Chemical Reaction Engineering, fifth ed., Pearson, Boston, 2016.
[53] E.B. Nauman, Chemical Reactor Design, Optimization, and Scaleup, second ed., John Wiley & Sons, Hoboken, NJ, 2008.
[54] M. Kaya, PFR_MeOH: Plug flow reactor model for methanol synthesis, 2025, GitHub repository, https://github.com/mertcnkaya/PFR_MeOH.
[55] J.M. Coulson, J.F. Richardson, R.K. Sinnott, G. Towler, Chemical engineering design: Chemical engineering, volume 6, fourth ed., in: Coulson & Richardson's Chemical Engineering, Butterworth-Heinemann, Oxford, UK, 1999.
[56] V. deutscher Ingenieure, VDI-wärmeatlas, 11th ed., in: VDI-Buch, Springer, Berlin Heidelberg, 2013, http://dx.doi.org/10.1007/978-3-642-19981-3.
[57] W. Sutherland, The viscosity of gases and molecular force, Phil. Mag. 36 (223) (1893) 507–531.
[58] W. van Antwerpen, C.G. du Toit, P.G. Rousseau, A review of correlations to model the packing structure and effective thermal conductivity in packed beds of mono-sized spherical particles, Nucl. Eng. Des. 240 (7) (2010) 1803–1818, http://dx.doi.org/10.1016/j.nucengdes.2010.03.009.
[59] T. Zoppi, P. Popov, Confidence ensembles: Tabular data classifiers on steroids, Inf. Fusion 120 (2025) 103126, http://dx.doi.org/10.1016/j.inffus.2025.103126.
[60] H. Uddin, Confirming the statistically significant superiority of tree-based machine learning algorithms over their counterparts for tabular data, PLOS ONE 19 (4) (2024) 1–12, http://dx.doi.org/10.1371/journal.pone.0301541.
[61] F. Pedregosa, G. Varoquaux, A. Gramfort, V. Michel, B. Thirion, O. Grisel, M. Blondel, P. Prettenhofer, R. Weiss, V. Dubourg, J. Vanderplas, A. Passos, D. Cournapeau, M. Brucher, M. Perrot, É. Duchesnay, Scikit-learn: Machine learning in python, J. Mach. Learn. Res. 12 (85) (2011) 2825–2830, http://dx.doi.org/10.48550/arXiv.1201.0490.
[62] J. Qiu, An analysis of model evaluation with cross-validation: Techniques, applications, and recent advances, Adv. Econ. Manag. Political Sci. 99 (2024) 69–72, http://dx.doi.org/10.54254/2754-1169/99/2024OX0213.
[63] M. Kaya, ML_MeOH: Machine Learning for Methanol Reactor Modelling, 2026, https://github.com/mertcnkaya/ML_MeOH.